Cardiovascular Innovations and Applications

Vol. 9 (2024) 53
ISSN 2009-8618
DOI 10.15212/CVIA.2024.0034

RESEARCH ARTICLE

Genetic Analysis Reveals Key Regulatory Axis in Aortic Dissection: CBL Regulated by HOXB13 and microRNA-1321

Zhiteng Chen[1,2,a], Qingyuan Gao[1,2,a], Junxiong Qiu[3,a], Miaomiao Ge[1,2], Shaohua Wang[4], Cheng Liu[4], Maoxiong Wu[1,2], Wanbing He[1,2], Jingfeng Wang[1,2], Yangxin Chen[1,2] and Haifeng Zhang[1,2]

[1]*Department of Cardiology, Sun Yat-sen Memorial Hospital, Sun Yat-sen University, Guangzhou, Guangdong 510120, P.R. China*
[2]*Laboratory of Cardiac Electrophysiology and Arrhythmia in Guangdong Province, Guangdong 510120, P.R. China*
[3]*Department of Cardiovascular Surgery, Sun Yat-sen Memorial Hospital, Sun Yat-sen University, Guangzhou, Guangdong 510120, P.R. China*
[4]*Department of Cardiology, Guangzhou First People's Hospital, South China University of Technology, Guangzhou, Guangdong 510120, P.R. China*

Received: 7 January 2024; Revised: 2 April 2024; Accepted: 26 April 2024

Abstract

Background: Aortic dissection (AD) is a fatal cardiovascular disease for which the key involved genes are largely unknown. Here, we aimed to identify promising AD biomarkers from high-throughput RNA expressing data.
Methods: In the GSE98770 dataset, differentially expressed mRNAs (DE-mRNAs) and microRNAs (DE-microRNAs) were identified through differentially expressed gene analysis and gene set enrichment analysis. The regulatory network between DE-mRNAs and DE-microRNAs was established, and hub genes were identified with Cytoscape. Relationships between hub genes and AD were confirmed in the Comparative Toxicogenomics Database (CTD). Potential key transcription factors were discovered with Cytoscape. Hub gene verification was performed by qPCR and immunofluorescence analyses of human specimens.
Results: DE-mRNAs and DE-microRNAs were identified. Four mRNAs and microRNA-1321 (miR-1321) were found to have the most connections with other genes. CBL was connected to the most genes and interacted with miR-1321, which was also connected to the most genes among the DE-microRNAs. In addition, CBL was associated with AD in the CTD. Among the top five transcription factors potentially regulating CBL transcription, only HOXB13 was a DE-mRNA. The findings were further successfully verified in human specimens.
Conclusion: CBL, which may be transcriptionally regulated by HOXB13 and post-transcriptionally regulated by miR-1321, was identified as the most promising potential biomarker for AD.

Keywords: aortic dissection; bioinformatics analysis; abstract homeobox b13; Cbl proto-oncogene; microRNA-1321

Introduction

Aortic dissection (AD) is a fatal cardiovascular disease associated with high mortality. AD is defined as the disruption of the medial layer provoked by intramural bleeding, thus resulting in separation of the aortic wall layers and subsequent formation of a true lumen and a false lumen, with or without communication [1]. The incidence rate of thoracic AD substantially varies, from 3 to 16 per 100,000

person-years [2]. AD remains a fatal disease, and more than 50% of affected individuals without proper treatment die during the acute phase of AD [3]. Although emergent treatments are performed, AD's rates of mortality, morbidity, and complications remain high [4, 5].

The mechanism of AD is not yet completely understood, but medial degeneration and inflammatory infiltration are both believed to be major underlying pathologic changes [6, 7]. Vascular smooth muscle cells (VSMCs) play a central role in medial degeneration. In the presence of AD risk factors, VSMCs show elevated secretory protein expression; diminished actin expression; and enhanced proliferation, migration, and production of metalloproteinases (MMPs) – changes referred to as the "phenotype switch." These changes lead to a switch in cell function from the regulation of vessel constriction and dilation to extracellular matrix deposition [8]. Apoptosis of VSMCs is another mechanism of medial degeneration. Preventing VSMC apoptosis with inhibitor treatment has been found to decrease AD incidence [9]. Beyond medial degeneration, inflammation is also critical in AD [6, 10]. Inflammatory infiltration in the media not only increases the expression of proteases and cell adhesion molecules, but also stimulates the release of reactive oxygen species, which jointly contribute to VSMC apoptosis and finally lead to medial degradation [11]. With the development of gene datasets and data mining, genetic associations with AD have received substantial attention [12]. Genetic discovery has extended understanding of AD, and multiple genes involved in AD have been verified and applied in clinical practice [13]. Thus, global genetic analysis is important for identifying genes involved in AD.

Although some gene expression profiling has been performed on human AD specimens, important genes might potentially have been missed because of a lack of global analysis. Regulatory network analysis provides substantial advantages in data mining [14]. Therefore, we constructed a microRNA-mRNA regulatory network by using a previously published dataset [15]. Hub genes in the network were identified, and their relationships with AD were confirmed in the Comparative Toxicogenomics Database (CTD). In addition, potential transcription factors (TFs) involved in regulating transcription of the hub mRNAs were searched. Finally, we performed experiments to verify the predictions. Through these approaches, we identified crucial differentially expressed genes (DEGs) in AD, and constructed a TF and post-transcriptional (microRNA) regulatory network. We further identified the Cbl proto-oncogene (CBL) and its regulation by abstract homeobox b13 (HOXB13) and microRNA-1321 (miR-1321) as key mechanisms in AD.

Methods

Gene Expression Omnibus Dataset

The GSE98770 dataset was downloaded from the NCBI Gene Expression Omnibus (GEO) database. This dataset includes six dissected aorta samples and five donor aorta samples, which were isolated from the intima-media layer of the dissected ascending aorta or from transplant donors [15]. Expression profiling arrays were generated with the GPL14550 Agilent-028004 SurePrint G3 Human GE 8×60K Microarray, and GPL17660 Agilent-031181 Unrestricted_Human_miRNA_V16.0_Microarray.

Screening of Differentially Expressed Genes and microRNAs

For DEG analysis, a sample cluster analysis with the hclust package in R was conducted, and samples with abnormal clusters were excluded from further analysis. The limma package in R was used to screen DEGs between dissected aorta samples and normal aorta samples in the dataset. The matrix of the expression profiling array was normalized by reads per kilobase of transcript per million mapped reads, 1 was added, and the values were was $\log_2$-transformed for subsequent analyses. Fold change (FC) values were calculated. Gene expression

[a]Zhiteng Chen, Qingyuan Gao and Junxiong Qiu contributed equally to this work and should be considered as co-first authors.

Correspondence: Jingfeng Wang, Yangxin Chen and Haifeng Zhang, Department of Cardiology, Sun Yat-sen Memorial Hospital, Sun Yat-sen University, Guangzhou, Guangdong 510120, China, Fax: +86-20-813-321-99, E-mail: wjingf@mail.sysu.edu.cn; chenyx39@mail.sysu.edu.cn; zhanghf9@mail.sysu.edu.cn

values with |FC| > 2 and adjusted P-value < 0.05 were used for filtering DEGs and differentially expressed microRNAs (DE-microRNAs).

Gene Set Enrichment Analysis

Gene set enrichment analysis (GSEA) was conducted to analyze the most significant and relevant pathways between dissected aorta and normal aorta samples. GSEA calculates an enrichment score (ES) for a pathway as the maximum value of the running sum, normalized to pathway size, thus yielding a normalized enrichment score (NES) reflecting the enrichment of the pathway in the list. Finally, a permutation-based P-value was computed and corrected for multiple testing to produce a permutation-based false-discovery rate (FDR) Q value ranging from 0 (highest significance) to 1 (no significance). Target pathways were selected according to rank with the FDR Q value threshold and NES [16].

mRNA-microRNA Network Construction and Hub Gene Identification

We used the miRTarbase [17], miRDB [18], TargetScan [19], and starBase v2.0 [20] online databases to predict potential microRNAs targeting DEGs. MicroRNAs found in any database were subjected to further analysis. We used Venn diagrams to select the target microRNAs from the microRNAs in common between the predicted microRNAs and DE-microRNAs. We then analyzed the correlation between the target microRNAs and DE-mRNAs in R and chose pairs with a negative correlation and a P-value <0.05.

The interaction network of DE-mRNAs was analyzed with the STRING database [21], which predicts protein functional associations and protein-protein interactions. Subsequently, for integration with the correlation of mRNAs and microRNAs analyzed above, we used Cytoscape software (V3.5.1) [22] to visualize microRNA-mRNA networks and determine hub genes.

Gene–Disease Relationship Analysis

We used the CTD to generate expanded networks, and predict novel associations among genes and disease phenotypes [23].

Investigation of Transcription Factors for Hub Genes

We used the plug-in iRegulon for Cytoscape software to search for TFs for hub genes, with parameters set to: (1) minimum identity between orthologous genes = 0.05; (2) maximum FDR for motif similarity = 0.001, and (3) NES ≥ 3.0 [24]. The top five regulators with the highest NES values were selected to construct the regulatory network.

Clinical Specimens for Verification

Dissected aorta specimens were collected from three patients with acute ascending aortic dissection undergoing surgical repair, whereas non-dissected aorta specimens were collected from three patients with coronary heart disease undergoing coronary artery bypass grafting. All patients were treated at Sun Yat-sen Memorial Hospital. The research was performed in accordance with the World Medical Association's Declaration of Helsinki, and all participants provided informed consent. The study protocol was approved by the institutional Ethics Committee of Sun Yat-sen Memorial Hospital.

Real-Time Quantitative Reverse Transcription PCR

Specimens were flash frozen in liquid nitrogen and ground into powder in an ultra-low temperature environment maintained with liquid nitrogen. Total RNA was isolated with RNAiso Plus Reagent (catalog No. 9109, Takara, Shiga-ken, Japan) according to the manufacturer's instructions. RNA was reverse transcribed with a Quantity Reverse Transcription Kit (catalog No. RR037A, Takara, Shiga-ken, Japan). Subsequently, qPCR assays were performed with SYBR Green reagent (catalog No. RR820B, Takara, Shiga-ken, Japan) under the following conditions: initial 30 s run at 95 °C before starting, followed by 95 °C for 5 s and 60 °C for 30 s for a total of 40 cycles. Primer sequences are listed in Supplementary Table 1.

Tissue Immunofluorescence Staining and Fluorescence In Situ Hybridization

The specimens were fixed with 4% paraformaldehyde solution, paraffin embedded, and prepared for

Table 1 Top Ten Pathways Selected by GSEA Ranking by NES.

Name	ES	NES	FDR
KEGG_TGF_BETA_SIGNALING_PATHWAY	0.1722	1.753354	0.007936508
KEGG_UBIQUITIN_MEDIATED_PROTEOLYSIS	0.114236	1.532394	0.011472276
KEGG_PATHWAYS_IN_CANCER	0.081834	1.601311	0.023715414
KEGG_STEROID_BIOSYNTHESIS	0.282671	1.467062	0.024299065
KEGG_VEGF_SIGNALING_PATHWAY	0.147537	1.477284	0.028409092
KEGG_MELANOMA	0.162422	1.562234	0.032608695
KEGG_JAK_STAT_SIGNALING_PATHWAY	0.097173	1.441833	0.034136545
KEGG_ACUTE_MYELOID_LEUKEMIA	0.180553	1.473516	0.056751467
KEGG_BIOSYNTHESIS_OF_UNSATURATED_FATTY_ACIDS	0.299062	1.551258	0.063097514

GSEA, gene set enrichment analysis; NES, normalized enrichment score; ES, enrichment score; FDR, false-discovery rate.

immunofluorescence (IF) staining. After dewaxing, the sections were hydrated with a graded alcohol series. The sections were treated with 0.5% Triton™ X-100 (catalog No. X100, Sigma-Aldrich, Missouri, USA), then subjected to antigen retrieval in sodium citrate solution in a microwave oven for 10 minutes.

For IF staining, the sections were incubated with specific antibodies at 4 °C overnight after blocking with 5% BSA. Target protein binding antibodies were visualized by incubation of sections with FITC or Alexa fluor®594 linked secondary antibodies.

For fluorescence in situ hybridization, sections were immersed in pre-hybridization solution for 30 minutes at 37 °C, then subjected to 1 hour hybridization with a probe against miR-1321 (sequence: ATCACATTCACCTCCCTGTT) at 37 °C. Sections were then washed in gradient SSC solutions.

Finally, the sections were incubated with DAPI solution (catalog No. 62248, Thermo Fisher Scientific, Massachusetts, USA) for 10 minutes and covered with coverslips. Fluorescence signals were captured with a fluorescence microscope as soon as possible. Antibodies and dilutions used for IF staining are provided in Supplementary Table 2.

Statistical Analyses

Data are expressed as mean ± SEM. Bioinformatics analyses were conducted in R software (version 3.5.0), and the statistical analyses of the experimental verification data were conducted in SPSS 19.0 (IBM, Illinois, USA). One-way ANOVA was used to analyze differences among multiple groups and was followed by SNK tests for multiple post hoc comparisons or Student's *t*-test for analysis of differences between two groups. The FDR method

Table 2 Correlation Analysis of Nine mRNA-microRNA Pairs.

Number	mRNA	MicroRNA	Correlation coefficient	P-value
1	CBL	hsa-miR-1207-5p	–0.86321	0.00272
2	CBL	hsa-miR-1321	–0.82309	0.00642
3	IL2RG	hsa-miR-1321	–0.86929	0.002334
4	PLA2G2A	hsa-miR-1321	–0.83441	0.005154
5	KRAS	hsa-miR-193a-3p	–0.72127	0.028296
6	KRAS	hsa-miR-199a-5p	–0.79022	0.011263
7	CBL	hsa-miR-199b-5p	–0.87345	0.002093
8	TYK2	hsa-miR-2861	–0.85826	0.003065
9	AMH	hsa-miR-3196	–0.83307	0.005293

CBL, Cbl proto-oncogene; IL2RG, interleukin 2 receptor subunit gamma; PLA2G2A, phospholipase A2 group IIA; TYK2, tyrosine kinase 2; KRAS, KRAS proto-oncogene, GTPase; AMH, anti-Mullerian hormone.

was used for P-value adjustment. A P-value <0.05 indicated statistical significance.

Results

Identification of Significant DEGs

To identify the most significant DEGs, we performed DEG analysis with the limma package and GSEA. Only genes identified by both methods were accepted as DEGs. The analysis flowchart is shown in Figure 1.

Sample cluster analysis indicated that all samples could be classified into two main clusters, except GSM2611536 and GSM2611540, which did not meet the inclusion criteria. The heatmap with data in the two main clusters was generated (heatmap of the top 100 genes in Figure 2A). Principal component analysis indicated satisfactory distinguishing ability for the different groups (Figure 2B). A volcano plot displayed the trend and fold change for all DEGs (Figure 2C). On the basis of our screening criteria, a total of 1471 genes, including 1366 up-regulated and 105 down-regulated genes, were identified between AD and normal aorta, and were identified as target DEGs.

GSEA identified 10 pathways involving 727 genes. Among them, three pathways were closely correlated with AD: the JAK-STAT pathway, transforming growth factor-β (TGF-β) pathway, and vascular endothelial growth factor (VEGF) pathway. The 289 genes in these three pathways were subsequently analyzed (Table 1, Figure 2D). Among them, 18 genes were identified among the target DEGs and were included in the following analyses (Figure 2E).

We next identified differentially expressed microRNAs (DE-microRNAs) to investigate post-transcriptional regulation. DE-microRNA analysis with the limma package revealed a total of 43

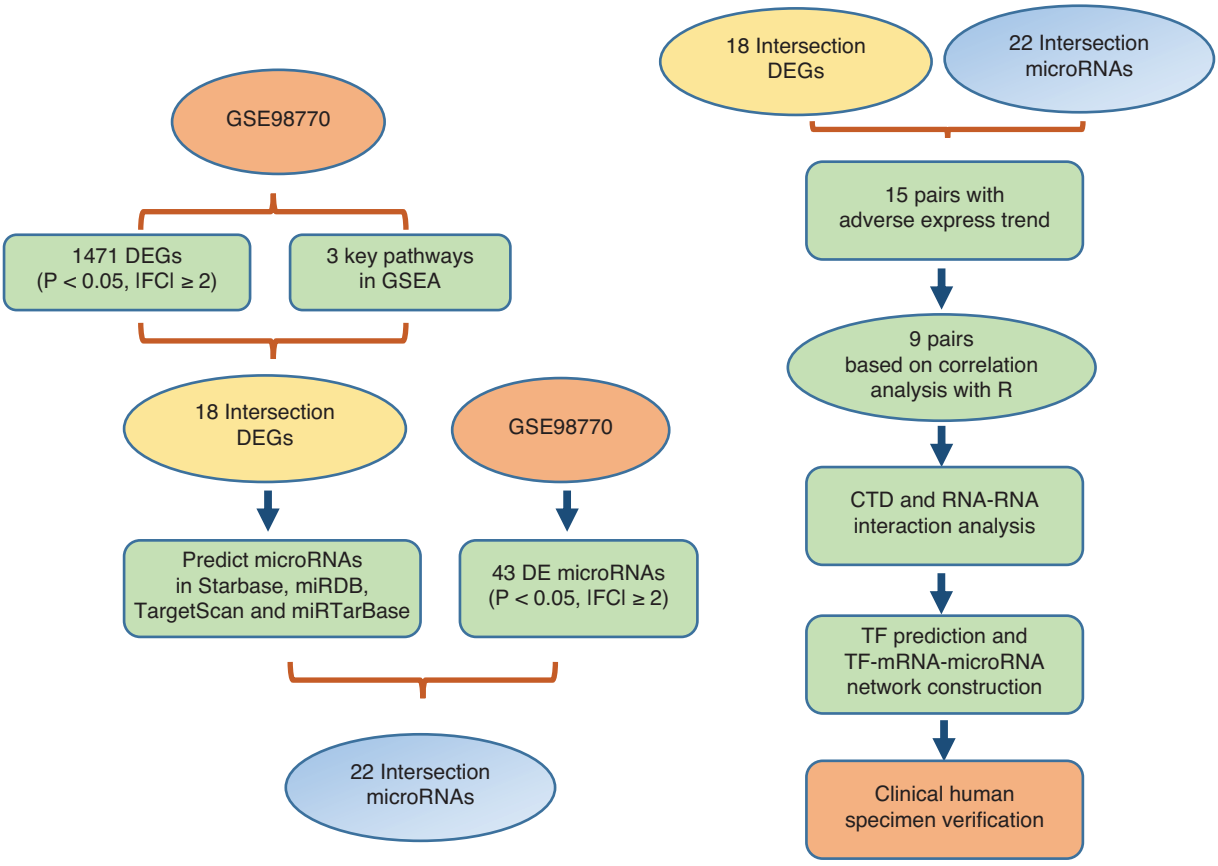

Figure 1 Flowchart of the Analysis Strategy.
DEGs, differentially expressed genes; DE microRNAs, differentially expressed microRNAs; CTD, Comparative Toxicogenomics Database; TF, transcription factor; |FC|, absolute value of the fold change.

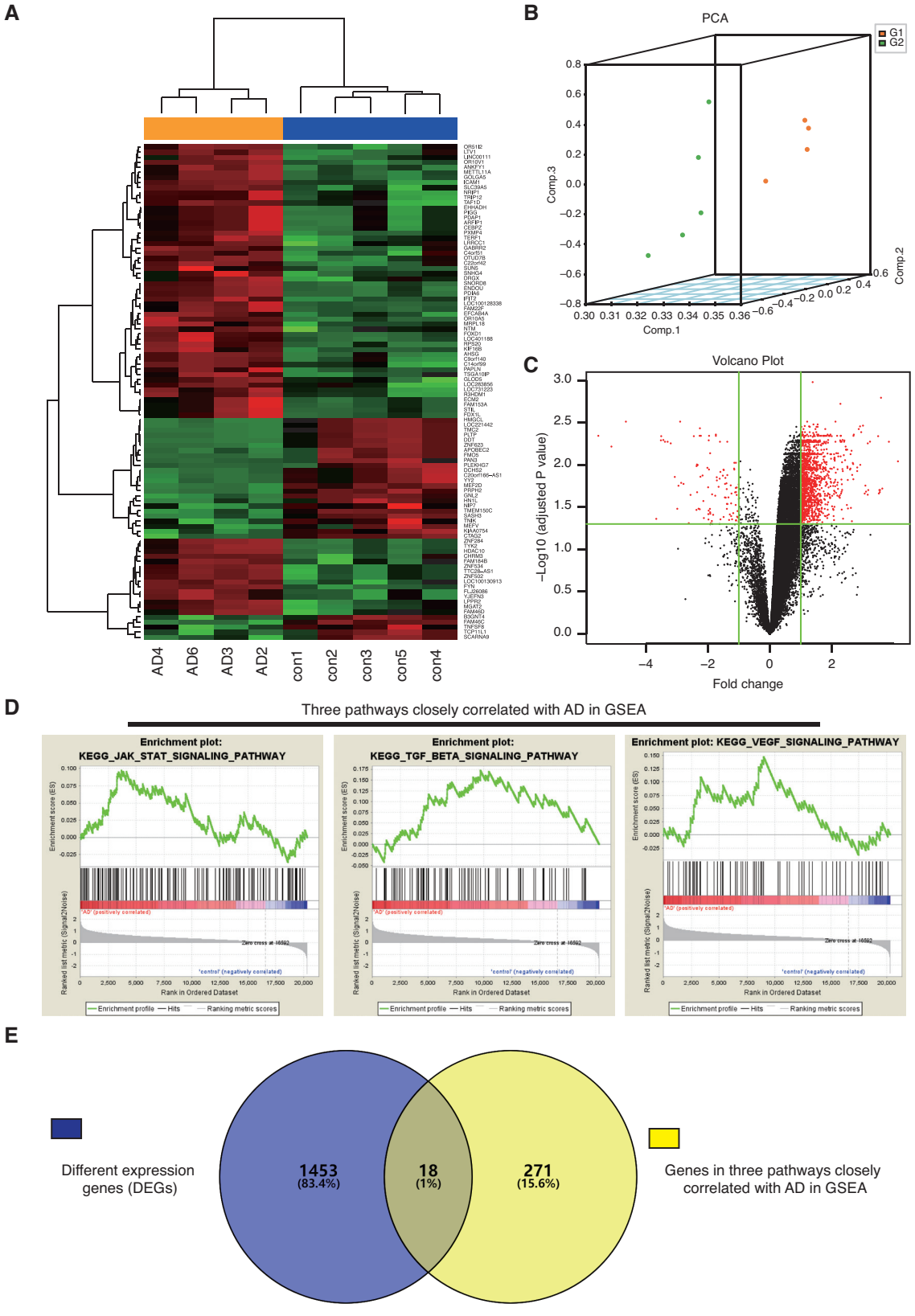

Figure 2 Identification of Significant DEGs in the GSE98770 Dataset.
A-C. Heat map and cluster analysis (A), principal component analysis (PCA) (B), and volcano plot (C) of the expression profile. D. Three pathways associated with aortic dissection, analyzed by GSEA. E. Venn diagram showing intersection between DE-mRNAs and mRNAs in the three pathways enriched in GSEA. GSEA, gene set enrichment analysis; DEGs, differentially expressed genes; DE-mRNAs, differentially expressed mRNAs.

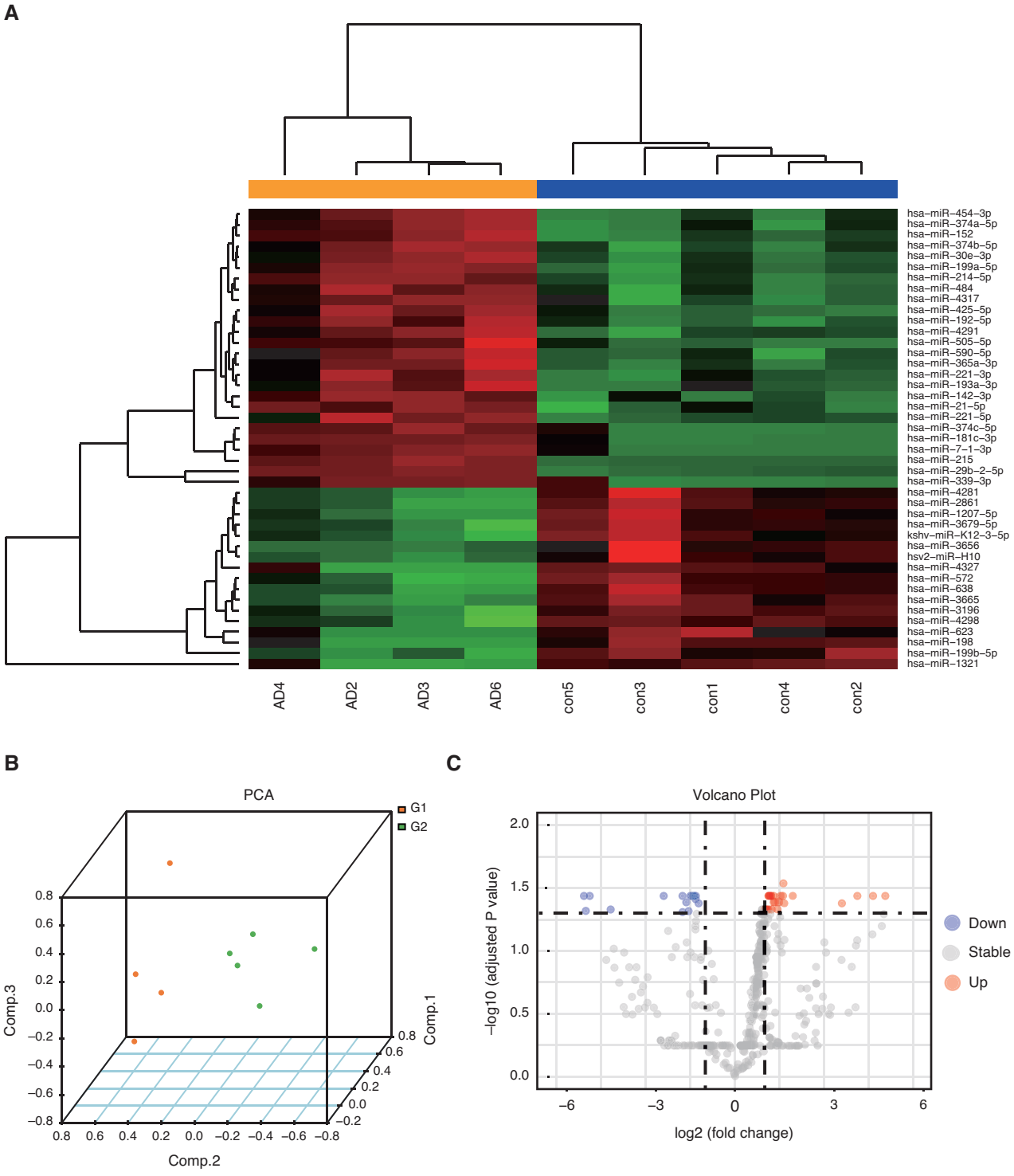

Figure 3 Identification of Significant DE-microRNAs in the GSE98770 Dataset.
A-C. A Heat map and cluster analysis (A), principal component analysis (PCA) analysis (B), and volcano plot (C) of the expression profile. DE-microRNAs, differentially expressed microRNAs.

DE-microRNAs (Figure 3A, B), and a volcano plot was constructed to display their trends and fold changes. A total of 26 microRNAs were up-regulated, and 17 microRNAs were down-regulated (Figure 3C).

Analysis of Correlations among DE-mRNAs, DE-microRNAs, and Hub Genes

The relationships between the DE-mRNAs and DE-microRNAs were explored. First, microRNAs

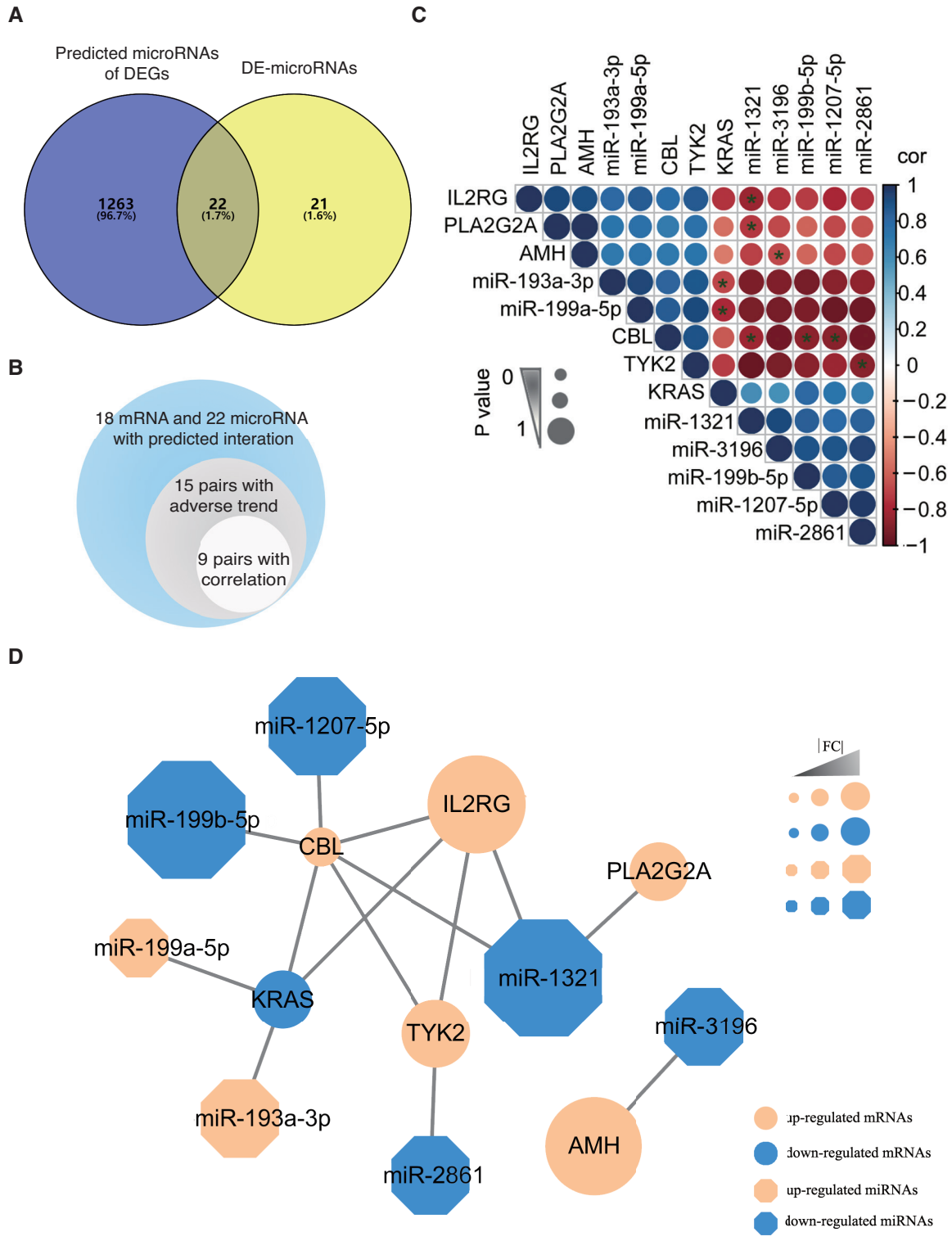

Figure 4 mRNA-microRNA Network Construction and Hub Gene Identification.
A. Venn diagram showing intersection between DE-microRNAs and predicted microRNAs from the DE-mRNAs. B. Hub mRNA-microRNA screening strategy. C. Correlation analysis of the six mRNAs and seven microRNAs. Cor, correlation coefficient. Blue shows positive correlation, and red shows negative correlation. Circle size represents the P-value of the correlation analysis. Larger spots indicate higher P-values. *, mRNA-microRNA pairs with predicted interaction and $P < 0.05$. D. Hub mRNA and microRNA analysis in Cytoscape. Circles represent mRNAs. Polygons represent microRNAs. Orange indicates up-regulation, and blue indicates down-regulation. Larger spots indicate higher absolute value of the fold change. CBL, Cbl proto-oncogene; IL2RG, interleukin 2 receptor subunit gamma; PLA2G2A, phospholipase A2 group IIA; TYK2, tyrosine kinase 2; KRAS, KRAS proto-oncogene, GTPase; AMH, anti-Mullerian hormone; |FC|, absolute value of the fold change.

potentially binding the 18 mRNAs of DEGs were predicted with public databases, and 1285 microRNAs were retrieved. Among them, 22 DE-microRNAs were identified and subjected to further analyses (Figure 4A). Because most microRNAs were negatively regulated, we sought to determine significant mRNA-microRNA pairs. A total of 15 mRNA-microRNA pairs showed negative regulation but only nine showed statistical significance (Figure 4B). The mRNAs and microRNAs in the nine mRNA-microRNA pairs, and their respective relative correlation coefficients and P-values, are summarized in Table 2 and Figure 4C. Six DE-mRNAs and seven DE-microRNAs were included. MiR-1321 targeted three mRNAs (CBL; interleukin 2 receptor subunit gamma, IL2RG; and phospholipase A2 group IIA, PLA2G2A), whereas the other microRNAs targeted only one mRNA (Figure 4C and Table 2). CBL was found to be targeted by three microRNAs (miR-1207-5p, miR-1321, and miR-199b-5p). The KRAS proto-oncogene, GTPase (KRAS) was targeted by both miR-193a-3p and miR199b-5p. The other mRNAs were targeted by only one microRNA.

According to these results, we continued to explore hub genes by building an mRNA-microRNA network *via* the STRING database and visually presenting it by using Cytoscape software. As illustrated in Figure 4D, CBL, IL2RG, tyrosine kinase 2 (TYK2), and KRAS have the most connections to other DEGs, whereas anti-Mullerian hormone (AMH) and PLA2G2A were related to only one DEG. Of note, CBL had the highest degree score among these mRNAs and was considered the hub gene (Table 3).

Regarding DE-microRNAs, miR-1321 had the highest degree score, was connected to the most DEGs, and was considered the hub gene (Table 3). The fold change in miR-1321 was also the most significant among the DE-microRNAs. We used a box plot to visualize the expression levels of the six closely associated genes, including those with high degree scores (CBL, IL2RG, KRAS, TYK2, PLA2G2A, and has-miR-1321; Figure 5A). The CTD database also indicated the close relationships among these mRNAs and AD (Figure 5B).

Table 3 Correlation Analysis with CytoHubba in Cytoscape Software.

Name	Degree
CBL	6
KRAS	4
IL2RG	4
TYK2	3
hsa-miR-1321	3
PLA2G2A	1
hsa-miR-2861	1
hsa-miR-199b-5p	1
hsa-miR-199a-5p	1
hsa-miR-193a-3p	1
hsa-miR-1207-5p	1

CBL, Cbl proto-oncogene; IL2RG, interleukin 2 receptor subunit gamma; PLA2G2A, phospholipase A2 group IIA; TYK2, tyrosine kinase 2; KRAS, KRAS proto-oncogene, GTPase; AMH, anti-Mullerian hormone.

Investigation of Transcription Factors for Hub Genes

The above results depicted the post-transcriptional regulation of AD hub genes, but the transcriptional mechanisms remained unknown. We therefore continued to explore TFs that might be involved. The Cytoscape software plug-in iRegulon was used to search potential TFs for hub genes. The top five TFs with the highest NES values were Forkhead box C1 (FOXC1), CCCTC binding factor (CTCF), abstract homeobox b13 (HOXB13), ETS proto-oncogene 1 (ETS1), and caudal-type homeobox transcription factor 1 (CDX1). These TFs were considered potentially useful in the construction of the regulatory network (Figure 6A). Of these five TFs, only HOXB13 was differentially expressed between AD and the controls in the dataset. Therefore, we constructed a regulatory network to intuitively display the relationships of this TF with mRNAs and microRNAs (Figure 6B). CBL, which might be transcriptionally regulated by HOXB13 and post-transcriptionally regulated by miR-1321, was considered the most promising gene potentially involved in the mechanism of AD development.

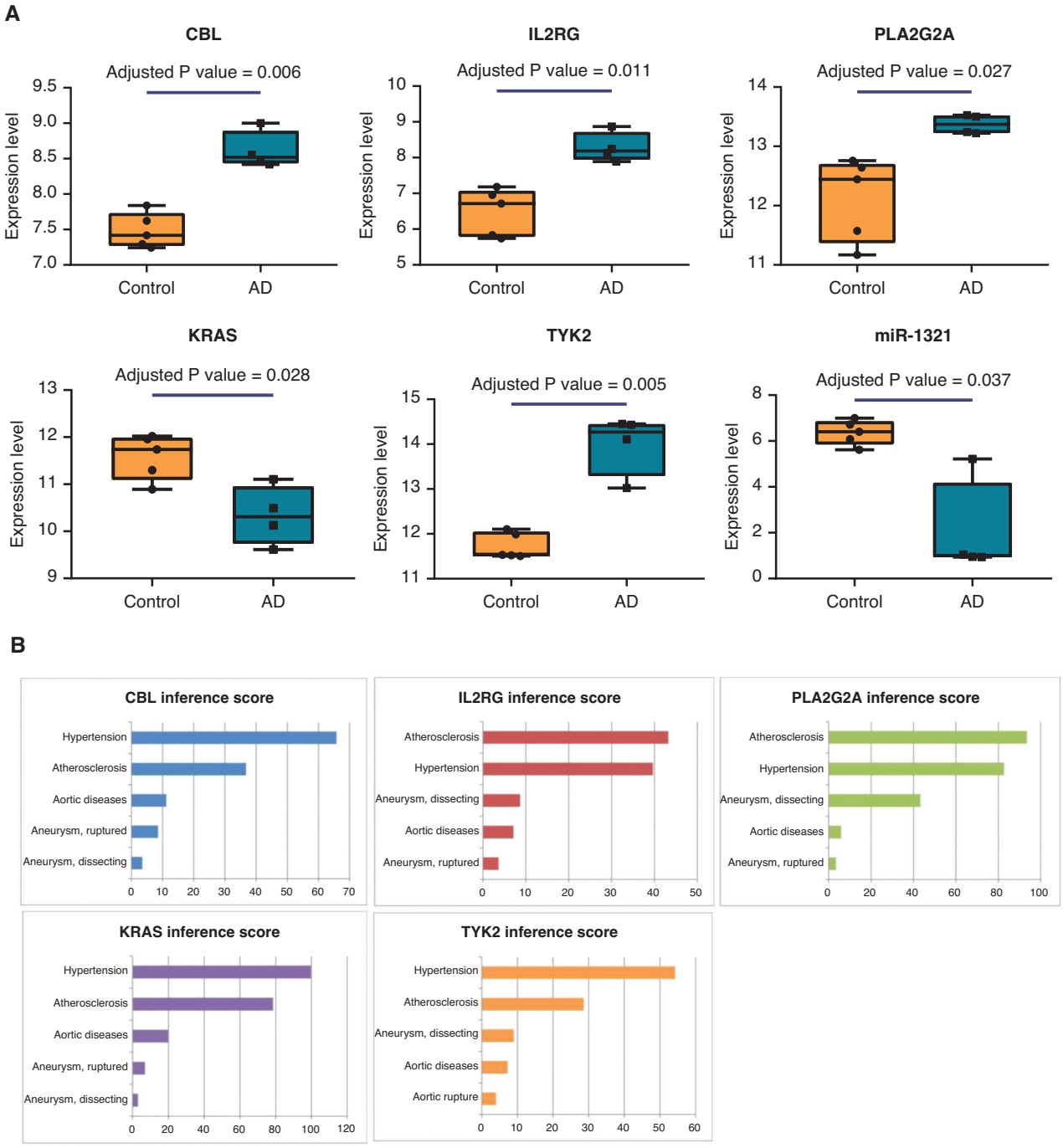

Figure 5 Hub mRNA-microRNA Expression and Functional Annotation by CTD.
A. Box plot of expression levels of the six closely associated genes CBL, IL2RG, KRAS, TYK2, PLA2G2A, and miR-1321. Adjusted P values were calculated with the limma package in R with Bayes tests. B. Associations between these genes and AD annotation with the CTD. CTD, Comparative Toxicogenomics Database; CBL, Cbl proto-oncogene; IL2RG, interleukin 2 receptor subunit gamma; PLA2G2A, phospholipase A2 group IIA; TYK2, tyrosine kinase 2; KRAS, KRAS proto-oncogene; miR-1321, microRNA-1321.

Validation of Hub Genes in Clinical Specimens

To validate the key regulatory axis identified above, we detected the expression of CBL, miR-1321, and HOXB13 in dissected and non-dissected aorta samples. Elastica van Gieson staining showed that the elastic fibers were intact with a regular arrangement in non-dissected aorta samples but were fractured and disordered in dissected aorta samples (Figure

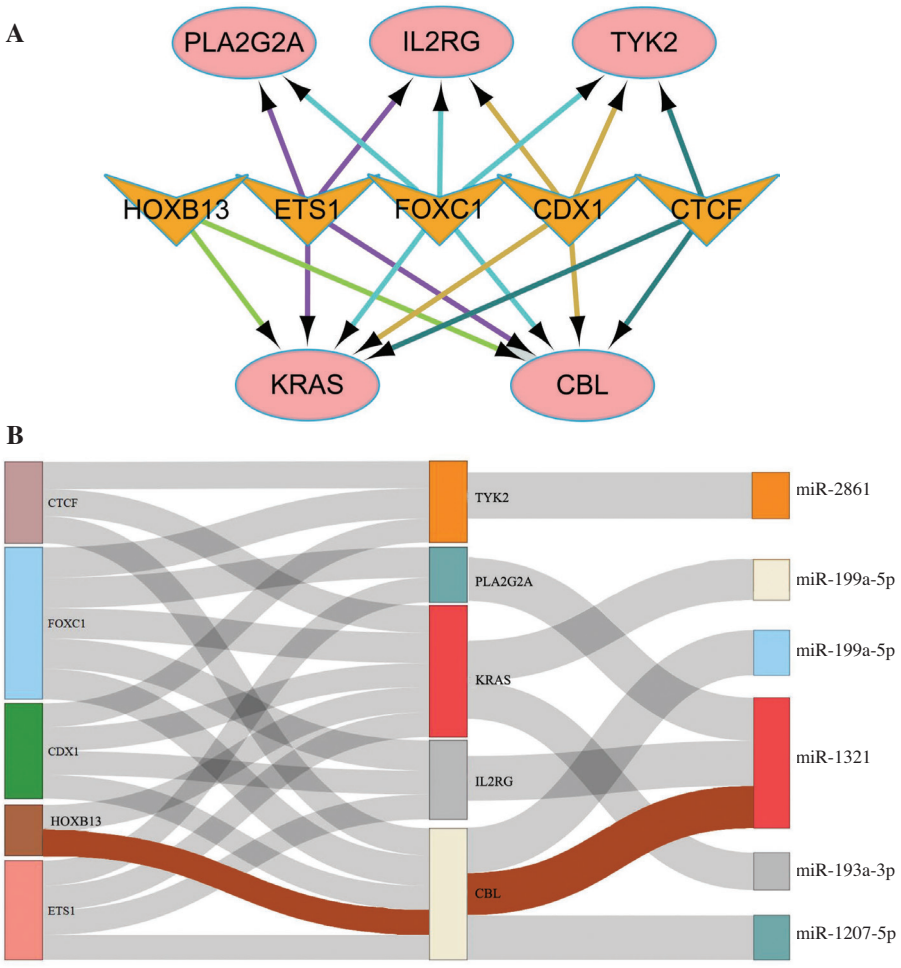

Figure 6 Transcription Factor Prediction and TF-mRNA-microRNA Network Construction.
A. Top five predicted transcription factors and their relationships with CBL, IL2RG, KRAS, TYK2, and PLA2G2A.
B. TF-mRNA-microRNA network construction. The brown line shows the key regulatory pathway HOXB13-CBL-miR-1321.
CBL, Cbl proto-oncogene; IL2RG, interleukin 2 receptor subunit gamma; PLA2G2A, phospholipase A2 group IIA; TYK2, tyrosine kinase 2; KRAS, KRAS proto-oncogene; miR, microRNA; FOXC1, Forkhead box C1; CTCF, CCCTC binding factor; HOXB13, abstract homeobox b13; ETS1, ETS proto-oncogene 1; CDX1, caudal-type homeobox transcription factor 1.

7A). Subsequently, qPCR showed increased expression of CBL and HOXB13, and decreased expression of miR-1321 in the dissected aorta samples, compared with the non-dissected aorta samples (Figure 7B). We also performed IF staining of CBL and HOXB13, and fluorescence in situ hybridization of miR-1321 in the aorta samples, and confirmed the same trends as those observed in qPCR (Figure 7C).

Discussion

Key molecules in AD development were largely unknown, and few studies had identified critical genes with altered expression among candidate genes through large scale analysis. We used bioinformatics analysis approaches to screen crucial genes during AD development from RNA-expression data.

Although similar research has been performed on the same dataset [15], we expected that more meaningful genes might be identified through our screening strategy. We searched key genes by constructing a regulatory network comprising the differentially expressed mRNAs and microRNAs, whereas the prior study identified genes mainly on the basis of a literature review. Although pathway analysis was also used in the prior study, some important genes might have been missing because of the lack of global analysis. Moreover, regulatory network analysis has substantial advantages in data mining, as shown our previous work [25].

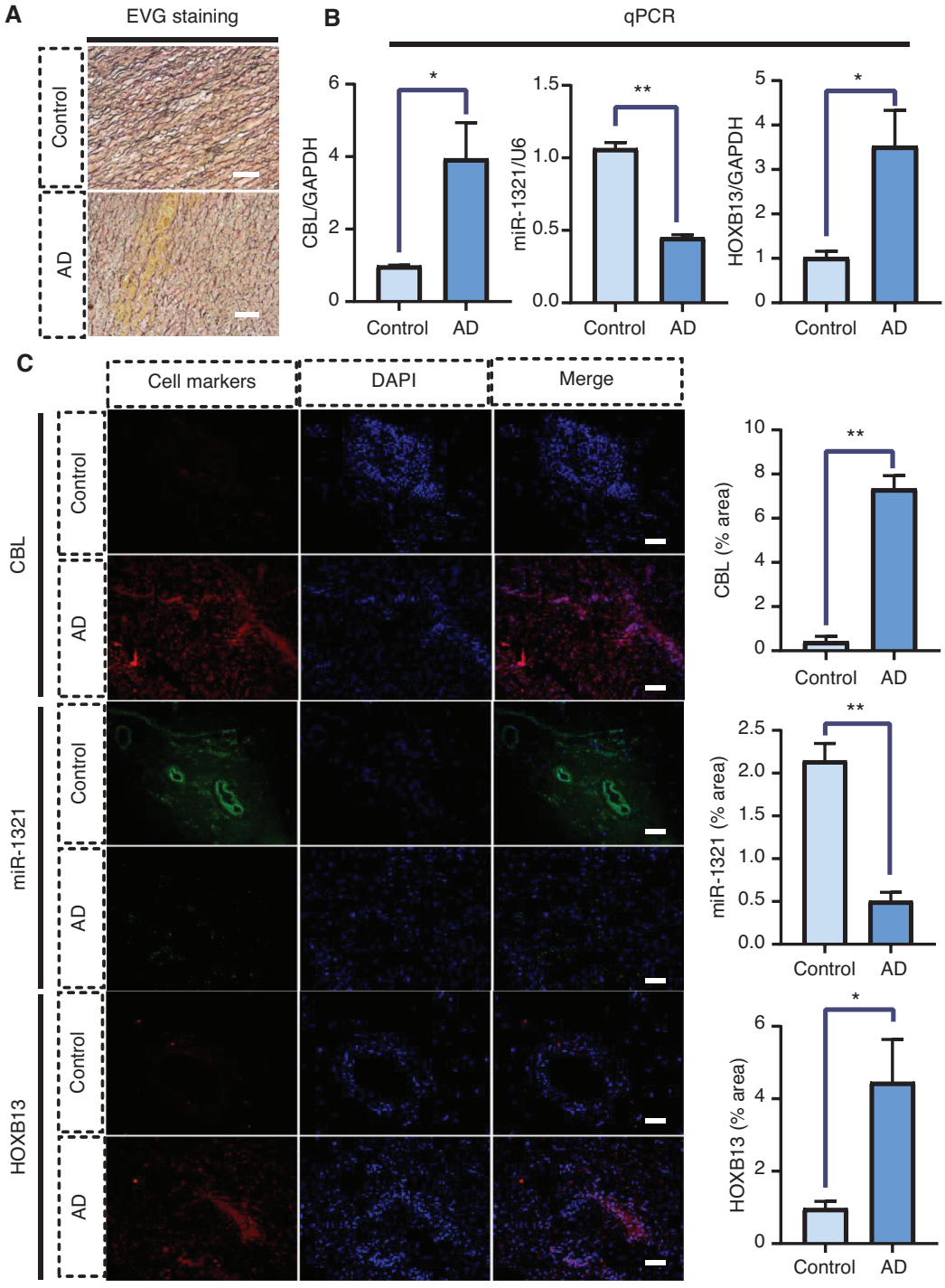

Figure 7 Validation of the Hub Genes in Clinical Specimens.
A. Elastica van Gieson (EVG) staining of dissected and non-dissected aorta samples. Black indicates elastic fibers, and red indicates collagen fibers. B. PCR detection of CBL, HOXB13, and miR-1321. C. Immunofluorescence staining (IF) of CBL and HOXB13 and fluorescence in situ hybridization (FISH) of miR-1321 in aorta samples. AD, aortic dissection; EVG, Elastica van Gieson; n = 3; *, $P < 0.05$; **, $P < 0.01$.

We identified CBL as a key hub gene associated with AD incidence, and suggested that it was the gene most plausibly involved in transcription and post-transcription regulation mechanisms.

CBL proteins are a highly conserved family of RING finger ubiquitin ligases that regulate signaling by tyrosine kinases in many pathways. CBL, a member of the CBL proteins, plays important roles

by mediating the ubiquitination of tyrosine kinases. The activation of CBL promotes myocyte apoptosis and exacerbates ischemia/reperfusion injury after myocardial infarction [26, 27]. Importantly, CBL has been demonstrated to participate in differentiation of cells including osteoclasts, adipocytes, and neural stem cells [28–30]. Although the potential role of CBL in AD development remains unclear, CBL has been shown to be important in VSMC differentiation. VSMC-derived neuropilin-like protein promotes the ubiquitination of platelet-derived growth factor receptor-β (PDGFR-β) in a CBL-dependent manner, thus regulating VSMC proliferation and secretion [31]. In addition, another study has demonstrated that increased tyrosine phosphorylation of CBL promotes the functions of platelet-derived growth factor-bb (PDGF-bb), which is widely believed to induce the VSMC phenotype switch [32], thus exacerbating vascular remodeling after vascular injury [33]. Therefore, despite a lack of direct evidence, current studies have suggested a potential role of CBL in AD development, on the basis of the critical role of VSMCs in AD. Consequently, further investigation is necessary.

MiR-1321 is not a frequently investigated microRNA, and its function remains unclear. Nevertheless, it has been reported to play important roles in both ovarian cancer and pediatric gliomas [34, 35]. Moreover, NEAT1 has been shown to regulate TJP3 expression by sponging miR-1321. Although miR-1321 has not been reported to participate in AD development, unlike miR-134-5p, miR-124, and miR-144-3p [36–38], it has been demonstrated to alleviate acute lung injury by targeting CXCR2 [39]. Interestingly, CXCR2 is among the most important inflammatory mediators in AD development, and anti-CXCR2 antibody treatment substantially ameliorates AD [40]. Therefore, beyond inhibition of CBL, miR-1321 might potentially regulate AD *via* CXCR2 suppression. Attention should also be paid to the potential regulation of ubiquitination process by miR-1321. According to bioinformatics prediction formulae [41], beyond CBL, a wide range of genes involved in ubiquitination process (e.g., ubiquitin related modifier 1, ubiquitin 4, ubiquitin-conjugating enzyme E2A, E2Q1 and E2V1, and E3 ubiquitin protein ligase family member 3) have been shown to be targeted by miR-1321. This finding also supports the possibility that miR-1321 might regulate CBL, which itself is a ubiquitination-regulating protein.

HOXB13 was the only TF among the DEGs and was predicted to regulate the hub mRNAs in the present study. Currently, no study has examined the relationship between HOXB13 and AD, but HOXB13 has been demonstrated to regulate cardiomyocyte maturation and the cell cycle [42]. Importantly, HOXB13 is crucial in collagen deposition. HOXB13 knockout mice exhibit high levels of collagen and elevated MMP-9, which are important markers of the VSMC phenotype switch and intra-lumen impairment of the aorta [43, 44]. HOXB13 also contributes to persistent inflammation [45], which also plays a key role in AD progression.

Notably, HOXB13 and microRNA-1321 are markers that can be measured in the serum or circulating cells [46, 47]. Thus, they may serve as promising biomarkers in future AD investigations. Further research is necessary to document the precise mechanisms of HOXB13, CBL, and miR-1321 during AD.

Some limitations of the present study should be acknowledged. First, although prior studies support the role of HOXB13-CBL-miR-1321 regulatory mechanism during AD incidence, we did not confirm such potential effects *in vivo*. Therefore, their functions remain unclear. Second, although current studies have strongly implicated CBL's effects on the VSMC phenotype switch, its role in inflammation during AD is unknown. Third, because gene expression in the dataset was obtained from gene microarrays, information was lacking regarding other unknown RNAs, particularly long non-coding RNAs and circular RNAs. We also did not explore changes in epigenetic modifications, which have been demonstrated to play important roles in AD development [48]. Finally, we explored only microRNAs that negatively regulated mRNAs. However, some microRNAs have been reported to activate mRNA translation [49, 50]. Therefore, some important microRNAs might have been neglected.

Despite the study's limitations, we identified that CBL's regulation by HOXB13 and microRNA-1321 constitutes the key regulatory axis in AD progression, according to bioinformatics analysis of high-throughput data. All genes had shared functions in the VSMC phenotype switch and/or inflammation,

both of which are key pathological processes in AD. A great need exists for further research to document the precise mechanisms of HOXB13, CBL and miR-1321 during AD. Moreover, RNA-sequencing techniques are necessary to provide a comprehensive gene expression profile that may reveal detailed mechanisms of AD.

Conclusion

CBL, which may be transcriptionally regulated by HOXB13 and post-transcriptionally regulated by miR-1321, was identified as the most promising potential biomarker for AD.

Highlights

We provided the following information in our present study.

1. Two approaches identifying differentially expressed mRNAs were applied to identify the most significant mRNAs.
2. MicroRNAs potentially targeting DE-mRNAs were predicted, and only those among the DE-microRNAs were included in the construction of an mRNA-microRNA interaction network.
3. On the basis of the network, CBL was identified as the hub gene. Interestingly, microRNA-1321, which also connected the most genes among the DE-microRNAs, was shown to target CBL.
4. Potential transcription factors for CBL were predicted, among which only HOXB13 was included in the DE-mRNA list.

Funding

This work was supported by grants from the Guangzhou Basic and Applied Basic Research Foundation (202201010940), National Natural Science Foundation of China (82200306), and Guangdong Basic and Applied Basic Research Foundation (2021A1515111092).

Acknowledgements

None.

Data Availability Statement

The dataset was downloaded from NCBI GEO (https://www.ncbi.nlm.nih.gov/geo/query/acc.cgi?acc=GSE98770). The data used and analyzed during the current study are available from the corresponding author on reasonable request.

Author Contributions

Zhiteng Chen, Qingyuan Gao, and Junxiong Qiu were responsible for most of the experiments. Maoxiong Wu, Shaohua Wang, and Wanbing He provided experimental assistance. Miaomiao Ge, and Cheng Liu helped with bioinformatics analyses. Haifeng Zhang, Yangxin Chen, and Jingfeng Wang designed and directed the study. All authors have read and approved the final submitted manuscript.

Conflicts of Interest

The authors declare no conflicts of interest.

Information on Ethics Committee Approval and Informed Consent

The research was performed in accordance with the World Medical Association's Declaration of Helsinki, and all participants provided informed consent. The study protocol was approved by the institutional Ethics Committee of Sun Yat-sen Memorial Hospital (ethics committee decision date: May 11, 2020; decision number: SYSEC-KY-KS-2020-076).

Consent for Publication

Not applicable.

Supplementary Material

Supplementary material for this paper can be found at https://cvia-journal.org/wp-content/uploads/2024/05/Revised_Supplementary_Material.pdf.

REFERENCES

1. Isselbacher EM, Preventza O, Hamilton Black J 3rd, Augoustides JG, Beck AW, Bolen MA, et al. 2022 ACC/AHA Guideline for the diagnosis and management of aortic disease: a report of the American Heart Association/American College of Cardiology Joint Committee on Clinical Practice Guidelines. Circulation 2022;146(24):e334–482.
2. Gouveia E Melo R, Mourão M, Caldeira D, Alves M, Lopes A, Duarte A, et al. A systematic review and meta-analysis of the incidence of acute aortic dissections in population-based studies. J Vasc Surg 2022;75(2):709–20.
3. Kim JB, Spotnitz M, Lindsay ME, MacGillivray TE, Isselbacher EM, Sundt TM 3rd. Risk of aortic dissection in the moderately dilated ascending aorta. J Am Coll Cardiol 2016;68(11):1209–19.
4. Silaschi M, Byrne J, Wendler O. Aortic dissection: medical, interventional and surgical management. Heart 2017;103(1):78–87.
5. Jia B, Luo C, Li C, Ge Y, Zhong Y, Qiao Z, et al. The anzhen risk scoring system for acute type A aortic dissection: a prospective observational study protocol. Cardiovasc Innov Appl 2023;7(1):e982.
6. Goldfinger JZ, Halperin JL, Marin ML, Stewart AS, Eagle KA, Fuster V. Thoracic aortic aneurysm and dissection. J Am Coll Cardiol 2014;64(16):1725–39.
7. Yang L, Wu H, Luo C, Zhao Y, Dai R, Li Z, et al. Urate-lowering therapy inhibits thoracic aortic aneurysm and dissection formation in mice. Arterioscler Thromb Vasc Biol 2023;43(6):e172–89.
8. Yang K, Ren J, Li X, Wang Z, Xue L, Cui S, et al. Prevention of aortic dissection and aneurysm via an ALDH2-mediated switch in vascular smooth muscle cell phenotype. Eur Heart J 2020;41(26):2442–53.
9. Chakraborty A, Li Y, Zhang C, Li Y, LeMaire SA, Shen YH. Programmed cell death in aortic aneurysm and dissection: a potential therapeutic target. J Mol Cell Cardiol. 2022;163:67–80.
10. Zhang Y, Zhang H, Zhao S, Qi Z, He Y, Zhang X, et al. S-nitrosylation of septin2 exacerbates aortic aneurysm and dissection by coupling the TIAM1-RAC1 axis in macrophages. Circulation 2024. https://doi.org/10.1161/CIRCULATIONAHA.123.066404.
11. Xia L, Sun C, Zhu H, Zhai M, Zhang L, Jiang L, et al. Melatonin protects against thoracic aortic aneurysm and dissection through SIRT1-dependent regulation of oxidative stress and vascular smooth muscle cell loss. J Pineal Res 2020;69(1):e12661.
12. Chou E, Pirruccello JP, Ellinor PT, Lindsay ME. Genetics and mechanisms of thoracic aortic disease. Nat Rev Cardiol 2023;20(3):168–80.
13. Renard M, Francis C, Ghosh R, Scott AF, Witmer PD, Adès LC, et al. Clinical validity of genes for heritable thoracic aortic aneurysm and dissection. J Am Coll Cardiol 2018;72(6):605–15.
14. Li Y, Du J, Liu B, She Q. Identifying key genes and related molecules as potential biomarkers in human dilated cardiomyopathy by comprehensive bioinformatics analysis. Cardiovasc Innov Appl 2023;8(1):e996.
15. Kimura N, Futamura K, Arakawa M, Okada N, Emrich F, Okamura H, et al. Gene expression profiling of acute type A aortic dissection combined with in vitro assessment. Eur J Cardiothorac Surg 2017;52(4):810–7.
16. Reimand J, Isserlin R, Voisin V, Kucera M, Tannus-Lopes C, Rostamianfar A, et al. Pathway enrichment analysis and visualization of omics data using g: Profiler, GSEA, Cytoscape and EnrichmentMap. Nat Protoc 2019;14(2):482–517.
17. Chou CH, Shrestha S, Yang CD, Chang NW, Lin YL, Liao KW, et al. miRTarBase update 2018: a resource for experimentally validated microRNA-target interactions. Nucleic Acids Res 2018;46(D1):D296–302.
18. Wong N, Wang X. miRDB: an online resource for microRNA target prediction and functional annotations. Nucleic Acids Res 2015;43(Database issue):D146–52.
19. Garcia DM, Baek D, Shin C, Bell GW, Grimson A, Bartel DP. Weak seed-pairing stability and high target-site abundance decrease the proficiency of lsy-6 and other microRNAs. Nat Struct Mol Biol 2011; 18(10):1139–46.
20. Li J, Liu S, Zhou H, Qu L, Yang J. StarBase v2.0: decoding miRNA-ceRNA, miRNA-ncRNA and protein-RNA interaction networks from large-scale CLIP-Seq data. Nucleic Acids Res 2014;42(Database issue):D92–7.
21. Szklarczyk D, Morris JH, Cook H, Kuhn M, Wyder S, Simonovic M, et al. The STRING database in 2017: quality-controlled protein-protein association networks, made broadly accessible. Nucleic Acids Res 2017;45(D1):D362–8.
22. Otasek D, Morris JH, Bouças J, Pico AR, Demchak B. Cytoscape automation: empowering workflow-based network analysis. Genome Biol 2019;20(1):185.
23. Davis AP, Grondin CJ, Johnson RJ, Sciaky D, McMorran R, Wiegers J, et al. The comparative toxicogenomics database: update 2019. Nucleic Acids Res 2019;47(D1):D948–54.
24. Janky R, Verfaillie A, Imrichová H, Van de Sande B, Standaert L, Christiaens V, et al. iRegulon: from a gene list to a gene regulatory network using large motif and track collections. PLoS Comput Biol 2014;10(7):e1003731.
25. Gao Q, Zhang H, Chen Z, Li Y, Wang S, Wen Z, et al. Construction and analysis of a ceRNA network in cardiac fibroblast during fibrosis based on in vivo and in vitro data. Front Genet 2021;11:503256.
26. Rafiq K, Kolpakov MA, Seqqat R, Guo J, Guo X, Qi Z, et al. c-Cbl inhibition improves cardiac function and survival in response to

myocardial ischemia. Circulation 2014;129(20):2031–43.
27. Yu S, Sun Z, Wang X, Ju T, Wang C, Liu Y, et al. Mettl13 protects against cardiac contractile dysfunction by negatively regulating C-Cbl-mediated ubiquitination of SERCA2a in ischemic heart failure. Sci China Life Sci 2023;66(12):2786–804.
28. Deepak V, Yang ST, Li Z, Li X, Ng A, Xu D, et al. IFT80 negatively regulates osteoclast differentiation via association with Cbl-b to disrupt TRAF6 stabilization and activation. Proc Natl Acad Sci U S A 2022;119(26):e2201490119.
29. Sekine Y, Kikkawa K, Honda S, Sasaki Y, Kawahara S, Mizushima A, et al. STAP-2 facilitates insulin signaling through binding to CAP/c-Cbl and regulates adipocyte differentiation. Sci Rep 2024;14(1):5799.
30. Vogt M, Unnikrishnan MK, Heinig N, Schumann U, Schmidt MHH, Barth K. c-Cbl regulates murine subventricular zone-derived neural progenitor cells in dependence of the epidermal growth factor receptor. Cells 2023;12(19):2400.
31. Guo X, Nie L, Esmailzadeh L, Zhang J, Bender JR, Sadeghi MM. Endothelial and smooth muscle-derived neuropilin-like protein regulates platelet-derived growth factor signaling in human vascular smooth muscle cells by modulating receptor ubiquitination. J Biol Chem 2009;284(43):29376–82.
32. Zhao Z, Wang Y, Li S, Liu S, Liu Y, Yu Y, et al. HSP90 inhibitor 17-DMAG effectively alleviated the progress of thoracic aortic dissection by suppressing smooth muscle cell phenotypic switch. Am J Transl Res 2019;11(1):509–18.
33. Tang Z, Wang Y, Fan Y, Zhu Y, Chien S, Wang N. Suppression of c-Cbl tyrosine phosphorylation inhibits neointimal formation in balloon-injured rat arteries. Circulation 2008;118(7):764–72.
34. Luo M, Zhang L, Yang H, Luo K, Qing C. Long non-coding RNA NEAT1 promotes ovarian cancer cell invasion and migration by interacting with miR-1321 and regulating tight junction protein 3 expression. Mol Med Rep 2020;22(4):3429–39.
35. Liu F, Xiong Y, Zhao Y, Tao L, Zhang Z, Zhang H, et al. Identification of aberrant microRNA expression pattern in pediatric gliomas by microarray. Diagn Pathol 2013;8:158.
36. Wang Y, Dong C, Peng G, Huang HY, Yu YS, Ji ZC, et al. MicroRNA-134-5p regulates media degeneration through inhibiting VSMC phenotypic switch and migration in thoracic aortic dissection. Mol Ther Nucleic Acids 2019;16:284–94.
37. Tang Y, Yu S, Liu Y, Zhang J, Han L, Xu Z. MicroRNA-124 controls human vascular smooth muscle cell phenotypic switch via Sp1. Am J Physiol Heart Circ Physiol 2017;313(3):H641–9.
38. Qi YF, Shu C, Xiao ZX. Post-transcriptional control of tropoelastin in aortic smooth muscle cells affects aortic dissection onset. Mol Cells 2018;41(3):198–206.
39. Liu S, Tang J, Huang L, Xu Q, Ling X, Liu J. Cordyceps militaris alleviates severity of murine acute lung injury through miRNAs-mediated CXCR2 inhibition. Cell Physiol Biochem 2015;36(5):2003–11.
40. Anzai A, Shimoda M, Endo J, Kohno T, Katsumata Y, Matsuhashi T, et al. Adventitial CXCL1/G-CSF expression in response to acute aortic dissection triggers local neutrophil recruitment and activation leading to aortic rupture. Circ Res 2015;116(4):612–23.
41. Agarwal V, Bell GW, Nam JW, Bartel DP. Predicting effective microRNA target sites in mammalian mRNAs. Elife 2015;4:e05005.
42. Nguyen NUN, Canseco DC, Xiao F, Nakada Y, Li S, Lam NT, et al. A calcineurin-Hoxb13 axis regulates growth mode of mammalian cardiomyocytes. Nature 2020;582(7811):271–6.
43. Shahmansouri N, Alreshidan M, Emmott A, Lachapelle K, Cartier R, Leask RL, et al. Evaluating ascending aortic aneurysm tissue toughness: dependence on collagen and elastin contents. J Mech Behav Biomed Mater 2016;64:262–71.
44. de Figueiredo Borges L, Jaldin RG, Dias RR, Stolf NA, Michel JB, Gutierrez PS. Collagen is reduced and disrupted in human aneurysms and dissections of ascending aorta. Hum Pathol 2008;39(3):437–43.
45. Mack JA, Maytin EV. Persistent inflammation and angiogenesis during wound healing in K14-directed Hoxb13 transgenic mice. J Invest Dermatol 2010;130(3):856–65.
46. Halabi S, Guo S, Park JJ, Nanus DM, George DJ, Antonarakis ES, et al. The Impact of circulating tumor cell HOXB13 RNA detection in men with metastatic castration-resistant prostate cancer (mCRPC) treated with abiraterone or enzalutamide. Clin Cancer Res 2024;30(6):1152–9.
47. Le TAH, Lao TD. Circulating microRNAs as the potential diagnostic and prognostic biomarkers for nasopharyngeal carcinoma. Genes (Basel) 2022;13(7):1160.
48. Tao Y, Li G, Yang Y, Wang Z, Wang S, Li X, et al. Epigenomics in aortic dissection: from mechanism to therapeutics. Life Sci 2023;335:122249.
49. Fabian MR, Sonenberg N, Filipowicz W. Regulation of mRNA translation and stability by microRNAs. Annu Rev Biochem 2010;79:351–79.
50. Ørom UA, Nielsen FC, Lund AH. MicroRNA-10a binds the 5'UTR of ribosomal protein mRNAs and enhances their translation. Mol Cell 2008;30(4):460–71.